CMB *B* polarization to map the large-scale structures of the universe

K. Benabed and F. Bernardeau
Service de Physique Théorique, Centre d'Etudes de Saclay, 91191 Gif-Sur-Yvette, France

L. van Waerbeke
Canadian Institut for Theoretical Astrophysics, 60 St. Georges Street, Toronto, Ontario, Canada M5S 3H8
(Received 30 March 2000; published 18 January 2001)

We explore the possibility of using *B*-type polarization of the cosmic microwave background to map the large-scale structures of the Universe taking advantage of the lens effects on the CMB polarization. The functional relation between the *B* component with the primordial CMB polarization and the line-of-sight mass distribution is explicated. Noting that a sizable fraction (at least 40%) of the dark halo population which is responsible for this effect can also be detected in a galaxy weak lensing survey, we present statistical quantities that should exhibit a strong sensitivity to this overlapping. We stress that it would be a sound test of the gravitational instability picture, independent of many systematic effects that may hamper lensing detection in CMB or a galaxy survey alone. Moreover, we estimate the intrinsic cosmic variance of the amplitude of this effect to be less than 8% for a 100 deg^2 survey with a $10'$ CMB beam. Its measurement would then provide us with an original means for constraining the cosmological parameters, more particularly, as it turns out, the cosmological constant Λ.

DOI: 10.1103/PhysRevD.63.043501 PACS number(s): 98.80.Es, 98.35.Ce, 98.62.Sb, 98.70.Vc

I. INTRODUCTION

In the new era of precision cosmology we are entering, forthcoming experiments will provide us with accurate data on cosmic microwave background (CMB) anisotropies [1]. This should lead to accurate determinations of the cosmological parameters, provided the large-scale structures of the Universe indeed formed from gravitational instabilities of initial adiabatic scalar perturbations. It was quickly realized, however, that even with the most precise experiments, the cosmological parameter space is degenerate when the primary CMB anisotropies alone are considered [2]. Complementary data that may be subject to more uncontrollable systematics are thus required, such as supernova surveys [3] (but see [4]) or constraints derived from the large-scale structure properties. Among the latter, weak lensing surveys are probably the safer [5], but still have not yet proved to be accurate enough with present day observations.

Secondary CMB anisotropies (i.e., induced by a subsequent interaction of the photons with the mass or matter fluctuations) offer opportunities for raising this degeneracy. Lens effects [6] are particularly attractive since they are expected to be one of the most important. They also are entirely driven by the properties of dark matter fluctuations, the physics of which involves only gravitational dynamics, and are therefore totally controlled by the cosmological parameters and not by details of galaxy or star formation rates. More importantly an unambiguous detection of lens effects on CMB maps would be a precious confirmation of the gravitational instability picture. Methods to detect lens effects on CMB maps have been proposed recently. High-order correlation functions [7], peak ellipticities [8], or large-scale lens-induced correlators [9,10] have been proposed for detecting such effects. All of them are, however, very sensitive to cosmic variance since lens effects are only a subdominant alteration of the CMB temperature patterns. The situation is different when one considers polarization properties. The reason is that in standard cosmological models temperature fluctuations at a small scale are dominated by scalar perturbations. Therefore the pseudoscalar part, the so-called *B* component, of the polarization is negligible compared to its scalar part (the *E* component) and can only be significant when CMB lens couplings are present. This mechanism was recognized in earlier papers [11,12,10]. The aim of this paper is to study systematically the properties of the lens-induced *B* field and uncover its properties.

In Sec. II, we perturbatively compute the lens effect on the CMB polarization *E* and *B* fields. This first order equation is illustrated by numerical experiments. The possibility of direct reconstruction of the projected mass distribution is also examined. As has already been noted a significant fraction of the potential wells that deflect the CMB photons can actually be mapped in local weak lensing surveys [13,14]. This feature has been considered so far in relation to the CMB temperature fluctuations. We extend in Sec. III these studies to the CMB polarization, exploiting the specificities of the field found in the previous section. In particular we propose two quantities that can be built from weak lensing and cosmic microwave background polarization surveys, the average value of which does not vanish in presence of CMB lens effects. Compared to a direct analysis of the CMB polarization, such tools have the joint advantage of being less sensitive to systematics—systematic errors coming from CMB mapping on the one hand and weak lensing measurement on the other have no reason to correlate—and so emerge even in presence of noisy data and of being an efficient probe of the cosmological constant. Indeed the expected amplitude of correlation is directly sensitive to the relative length of the optical bench, from the galaxy source plane to the CMB plane, which is mainly sensitive to the

cosmological constant. Filtering effects and cosmic variance estimation of such quantities are considered in this section as well.

II. LENS EFFECTS ON CMB POLARIZATION

A. First order effect

Photons emerging from the last scattering surface are deflected by the large-scale structures of the Universe that are present on the lines of sight. Therefore photons observed from the apparent direction $\vec{\alpha}$ must have left the last scattering surface from a slightly different direction, $\vec{\alpha}+\vec{\xi}(\vec{\alpha})$, where $\vec{\xi}$ is the lens-induced apparent displacement at that distance. The displacement field is related to the angular gradient of the projected gravitational potential:

$$\xi_i(\vec{\alpha}) = -\frac{2}{c^2}\int^{z_s} \mathrm{d}z \frac{D_{z\to z_s}}{D_z D_{z_s}} \Phi_{,i}(\vec{\alpha},z), \tag{1}$$

where $\Phi_{,i}$ is the angular gradient of the gravitational potential in the direction orthogonal to the line of sight, D is the angular distance, and z_s is the source plane. In the following, the lens effect will be described by the deformation effects it induces, encoded in the amplification matrix

$$\mathcal{A}^{-1} = \begin{pmatrix} 1-\kappa-\gamma_1 & -\gamma_2 \\ -\gamma_2 & 1-\kappa+\gamma_1 \end{pmatrix} = \delta_i^j + \xi^j_{,i}, \tag{2}$$

so that

$$\kappa = -\frac{1}{2}(\xi^x_{,x}+\xi^y_{,y}),$$

$$\gamma_1 = -\frac{1}{2}(\xi^x_{,x}-\xi^y_{,y}),$$

$$\gamma_2 = -\xi^y_{,x} = -\xi^x_{,y}. \tag{3}$$

All these fields can be written in terms of the second order derivatives of the projected potential. The lens effect affects the local polarization just by moving the apparent direction of the line of sight [16]. Thus, if we use the Stokes parameters Q and U to describe the local polarization vector

$$\vec{P} = \begin{pmatrix} Q \\ U \end{pmatrix},$$

we can relate the observed polarization $\hat{\vec{P}}$ to the primordial one by the relation

$$\hat{Q}(\vec{\alpha}) = Q(\vec{\alpha}+\vec{\xi}), \quad \hat{U}(\vec{\alpha}) = U(\vec{\alpha}+\vec{\xi}). \tag{4}$$

From now on we will denote $\hat{x}$ an observed quantity and x the primordial one. Since $\vec{\alpha}' = \vec{\alpha}+\vec{\xi}$ is the sky coordinate system for the observer, the amplification matrix $\mathcal{A}$ is also the Jacobian of the transformation between the source plane and the image plane. We will restrain here our computation to the weak lensing effect, so the observed quantity will not take into account any other secondary effect. It is very important at this point to note that the lensing effect does not produce any polarization or rotate the Stokes parameters. In this regime its effect reduces to a simple deformation of the polarization patterns, similar to the temperature maps. This is the mechanism by which the geometrical properties of the polarization field are changed.

To see that we have to consider the *electric* (E) and *magnetic* (B) components instead of the Stokes parameters. At small angular scales (we assume that a small fraction of the sky can be described by a plane), these two quantities are defined as

$$E \equiv \Delta^{-1}[(\partial_x^2-\partial_y^2)Q + 2\partial_x\partial_y U],$$

$$B \equiv \Delta^{-1}[(\partial_x^2-\partial_y^2)U - 2\partial_x\partial_y Q], \tag{5}$$

where Δ^{-1} refers here to the inverse of the Laplacian operator. These fields reflect the nonlocal geometrical properties of the polarization field. The electric component accounts for the scalar part of the polarization, and the magnetic one, the pseudoscalar part: by parity change E is conserved, whereas the B sign is changed. As has been pointed out in previous papers [11,12,15], lens effects partly redistribute the polarization power in these two fields.

We explicate this latter effect in the weak lensing regime where the distortion, κ and γ_i components are small. This is indeed expected to be the case when lens effects by the large-scale structures are considered, for which the typical value of the convergence field κ is expected to be $\sim 2\%$ at the $10'$ scale. The leading order effect is obtained by simply plugging Eq. (4) into Eq. (5) and by expanding the result at leading order in ξ, κ, and γ. Noting that, for any field X that is affected by the lensing effect (these calculations are very similar to those done in [14]),

$$\partial_i \hat{X} = \widehat{\partial_k X}\cdot(\delta_i^k + \xi^k_{,i}),$$

$$\partial_i\partial_j \hat{X} = \widehat{\partial_k\partial_l X}\cdot(\delta_i^k+\xi^k_{,i})(\delta_j^l+\xi^l_{,j}) + \widehat{\partial_k X}\cdot\xi^k_{,ij}, \tag{6}$$

we can write a perturbation description of the lensing effect on electric and magnetic components of the polarization. At leading order one obtains

$$\Delta\hat{E} = \Delta E + \xi^i\partial_i\Delta E - 2\kappa\Delta E - 2\delta_{ij}(\gamma^i\Delta P^j + \gamma^i_{,k}P^{j,k}) + O(\gamma^2),$$

$$\Delta\hat{B} = \Delta B + \xi^i\partial_i\Delta B - 2\kappa\Delta B - 2\epsilon_{ij}(\gamma^i\Delta P^j + \gamma^i_{,k}P^{j,k}) + O(\gamma^2), \tag{7}$$

where we used the fact that $\widehat{\Delta X} = \Delta X + \xi^i\partial_i\Delta X$ at the leading order. The formulas for E and B are alike. The only difference is in the δ_{ij} and ϵ_{ij} (the latter is the totally antisymmetric tensor, $\epsilon_{11}=\epsilon_{22}=0$, $\epsilon_{12}=-\epsilon_{21}=1$), which reflect the geometrical properties of the two fields. The first three terms

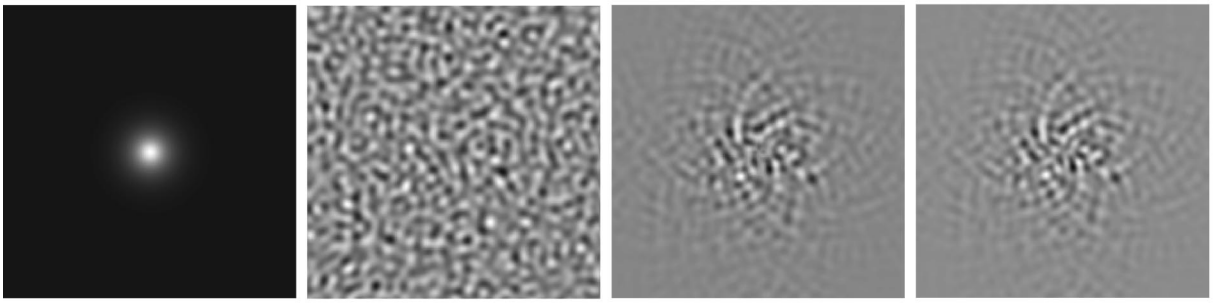

FIG. 1. Lens effect induced by a large isothermal sphere with finite core radius. The κ map of the lens is shown on left panel. The primordial *E* sky is presented in the middle left panel. It has been generated for a $\Omega_0=0.3$, $\Lambda=0.7$ model, without tensor modes. The middle right panel displays the true reconstructed $\Delta\hat{B}$ field in a 4.5×4.5 deg map and the right panel shows the first order approximation. Note that the rosettelike shape the eye seems to catch in *B* fields is a numerical coincidence and has no special significance.

of each of these equations represent the naive effect: the lens-induced deformation of the *E* or *B* field. This effect is complemented by an enhancement effect (respectively, $\kappa\Delta E$ and $\kappa\Delta B$) and by shear-polarization mixing terms. The latter effects consist of two parts: one, which we will call the Δ term, that couples the shear with the second derivative of the polarization field and the other one, hereafter the ∇ term, that mixes the gradient of the shear and polarization. In our previous work [14], terms similar to ∇ (i.e., in the gradient of the lens effect) had been neglected since they had a null contribution to the correlation coefficient we computed. This is no longer true here; we will indeed show later that Δ and ∇ terms have similar amplitudes.

One consequence of standard inflationary models on CMB anisotropies is the unbalanced distribution of power between the electric (E) and magnetic (B) components of its polarization. Adiabatic scalar fluctuations do not induce *B*-type polarization and they dominate at small scales over tensor perturbations (namely, the gravity waves). So even though gravity waves induce *E*- and *B*-type polarizations in a similar amount, the *primary* CMB sky is expected to be completely dominated by *E*-type polarization at small scales. Then for this class of models the actual magnetic component of the polarization field is generated by the corrective part of Eq. (7):

$$\Delta\hat{B}=-2\epsilon_{ij}(\gamma^i\Delta\hat{P}^j+\gamma^i_{,k}\hat{P}^{j,k}). \tag{8}$$

This result extends the direct lens effects described in Benabed and Bernardeau [12] who focused their analysis on the lens effect due to the discontinuity of the polarization field in case of cosmic strings. Previous studies of the weak lensing effect on the CMB showed that with lensing, the *B* component becomes important at small scales [17]. We obtain here the same result but with a different method. Equation (8) means that the polarization signal *P* is redistributed by the lensing effect in a way that breaks the geometrical properties of the primordial field. Note here that it is mathematically possible to build a shear field that preserves these geometrical properties and that does not create any *B* signal at small scales. We will discuss this problem in Sec. II C. It also means that *B* directly reflects the properties of the shear map. We will take advantage of this feature to probe the correlation properties of *B* with the projected mass distribution in the next sections.

B. Lens-induced *B* maps

We show examples of lens-induced *B* maps. These maps have been calculated using ''CMBSLOW'' code developed by Riazuelo (see [18]) to compute primordial polarization maps [we use realizations of standard cold dark matter (CDM) model to illustrate lens effects]. Then various shear maps are applied. We present both true distortions (obtained by Delaunay triangulation[1] used to shear the *Q* and *U* fields) and the first order calculations given by Eq. (8).

Figure 1 presents the shear effect induced by an isothermal sphere with finite core radius (and the lens edges have been suppressed by an exponential cutoff to minimize numerical noise). The agreement between true distortion (central panel) and the first order formula (right panel) is good. However, a close examination of the maps reveals that some structures in the true map are slightly wider than their counterparts in the first order map. This error is more severe in the center, where the distortion is bigger, which is to be expected since the limits of the validity region of first order calculations are reached.

For illustration sake, Fig. 2 shows the *B* field induced by a *realistic* distortion. We use second order Lagrangian dynamics [19] to create a 2.5×2.5 deg map that mimics a realistic projected mass density up to $z=1000$ and used its gravitational distortion to compute a typical weak lensing-induced *B* map. Again we compare the *exact* effect (i.e., the left panel where Delaunay triangulation is used) and the first order formula (middle panel). The right panel shows the dif-

[1]To perform the exact lensing effect on a CMB map, we compute the displacement field and the polarization fields on regular grids. Then the CMB grid is deformed according to Eq. (4) to shear the grid containing the CMB data. The resulting polarization fields are remapped onto a regular grid using Delaunay triangulation, which provides us with an efficient algorithm to interpolate irregularly sampled data on a discreet grid. The result is accurate down to the grid size.

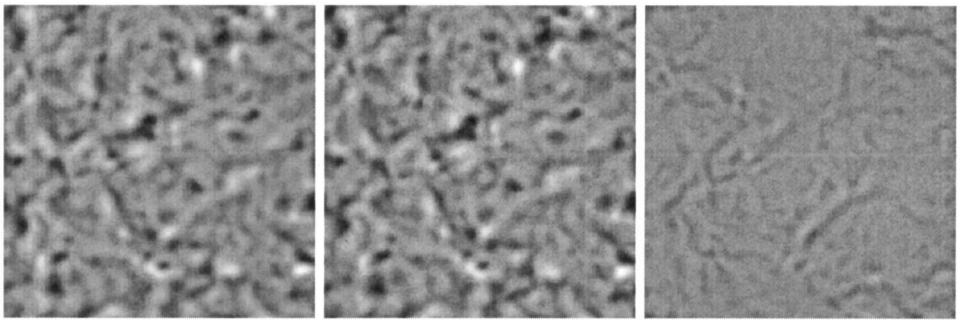

FIG. 2. The effect of a *realistic* weak lensing field on *B*. 2.2×2.2 deg survey with 1.8′ resolution. The left panel shows exact distortion obtained by Delaunay triangulation, the middle one, the first order formula result, and the right gives the difference between the two. The three panels share the same color table. The mean amplitude in the difference map is about 3 times smaller.

ference between the two maps. It reveals the locations where the two significantly disagree. In fact most disagreements are due to a slight mismatch of the *B* patch positions, which lead to dipolelike effects in this map.

We also show here a comparison of the two parts of the first order formula, Eq. (8), in order to see which of the Δ or ∇ terms dominates. It would be more comfortable if one of the two terms were dominant; however, Fig. 3 shows that it is not the case. Even if the Δ term dominates at low (<1000) l, it is only twice bigger than the ∇ one at this scale. The inverse is true for higher (3000–5000) l's. This can be seen by looking at Fig. 4 where we show the relative amplitudes of the Δ and ∇ contributions. The Δ part gives birth to large patches (around 10′) while the ∇ panel shows a lot more small features. Details of this calculations are given in the Appendix.

C. Direct reconstruction: The Kernel problem

The fact that the observable *B* is at leading order proportional to the weak lensing signal invites us to try a direct reconstruction, similar to the lensing mass reconstruction. In fact, we can write

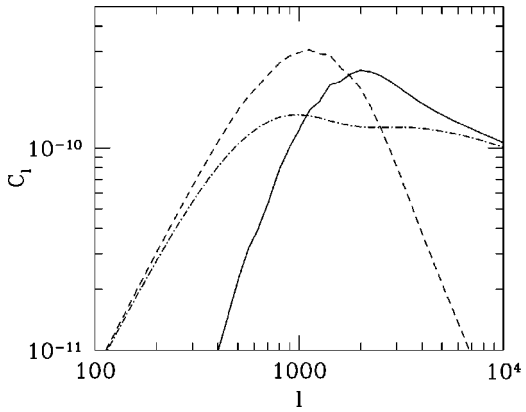

FIG. 3. The C_l of ΔB (solid line), the Δ term (dashed line), and the ∇ term (dot-dashed line). The Δ part is dominant at small l's, around $l=1000$, that is to say, for structures around 10′. The ∇ contribution gives birth to smaller structures in the 1–2 arc min range. The C_l curve is in good agreement with results presented previously in the literature [11,15].

$$\Delta\hat{B} = -2\epsilon_{ij}(\gamma^i \Delta\hat{P}^j + \gamma^i_{,k}\hat{P}^{j,k}) \equiv F[\gamma] \tag{9}$$

and our reconstruction problem becomes an inversion problem for the operator *F*. Unfortunately, one can prove that this problem has no unique solution. It is due to the fact that *F* admits a huge kernel, in the sense that, given a polarization map, there is a wide class of shear fields that will conserve a null *B* polarization. The demonstration of this property is sketched in the following.

Since the unlensed polarization is only electric in our approximation, we can describe it by the Laplacian of a scalar field:

$$E \equiv \Delta\varphi \quad \text{so} \quad \begin{cases} Q = (\partial_x^2 - \partial_y^2)\varphi, \\ U = 2\partial_x\partial_y\varphi. \end{cases} \tag{10}$$

The same holds for the shear and convergence fields

$$\kappa \equiv \frac{\Delta\psi}{2}, \quad \gamma_1 = \frac{1}{2}(\partial_x^2 - \partial_y^2)\psi, \quad \gamma_2 = \partial_x\partial_y\psi. \tag{11}$$

Thus we need to know, for a given φ field, whether there is any ψ that satisfies the equation

$$\gamma_2 \Delta Q - \gamma_1 \Delta U + \partial_i \gamma_2 \partial^i Q - \partial_i \gamma_1 \partial^i U = 0. \tag{12}$$

φ and ψ can be written as polynomial decompositions:

$$\varphi(x,y) = \sum_{n,l} a_{nl} x^n y^l,$$

$$\psi(x,y) = \sum_{m,k} b_{mk} x^m y^k. \tag{13}$$

Using Eqs. (13) in Eq. (12) we are left with a new polynomial whose coefficients c_{ij} are sums of $a_{nl} \times b_{mk}$ and have to be all put to zero. With the coefficient equations in hand, it is easy to prove that assuming all the b_{mk} coefficients up to $m+k=N$ are known and writing the equations $\forall\ i+j = (N+1)-3$, $c_{ij}=0$, we can compute out of all the a_{nl} all but three b_{mk} with $m+k=N+1$. This is somewhat similar to mass reconstruction problems from galaxy surveys where one cannot avoid the mass sheet degeneracy. The situation is, however, worse in our case since not only constant conver-

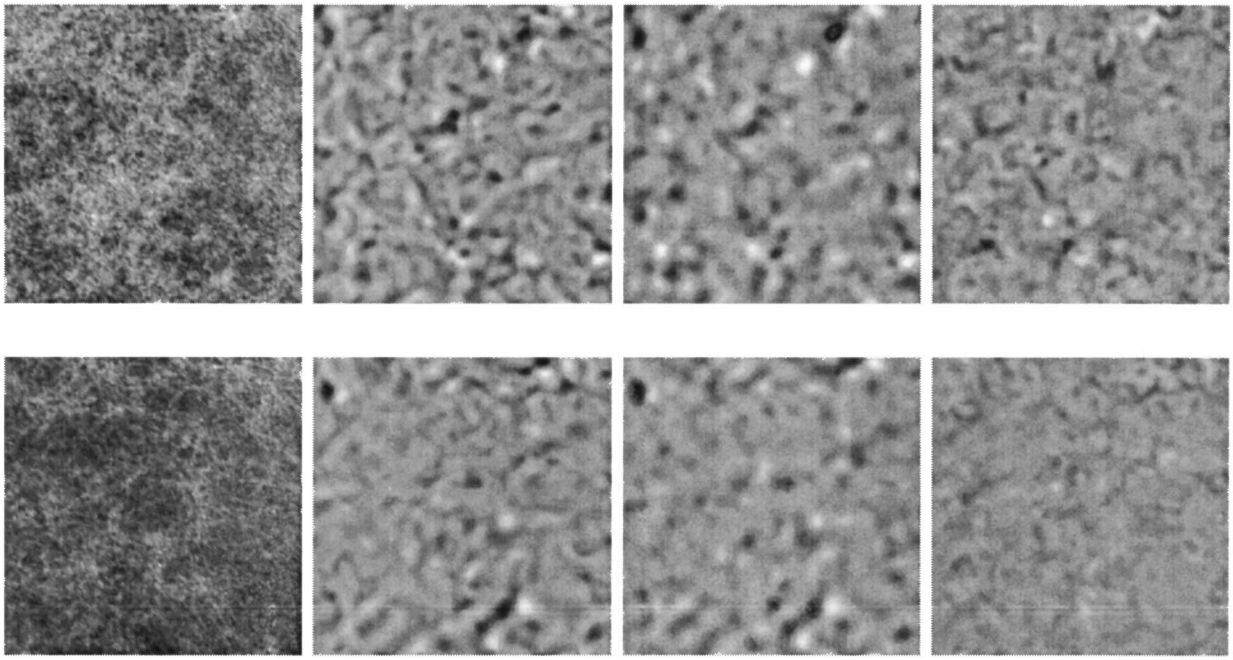

FIG. 4. The effect of the two terms of the perturbation formula. Top row, the lens effect is the sum of the lenses up to recombination. Bottom row, we use the same line-of-sight mass fluctuations but only up to redshift unity; it represents our ''local'' lensing survey. The convergence fields (left panels) have been computed by slicing the z axis and summing up the lensing effect in each slice. Lens-lens coupling (including departure from the Born approximation) terms have been neglected, which is consistent with our first order approximation. The convergence in each slice has been created by using second order Lagrangian dynamics. The middle-left panels show the leading order contribution, the middle right the Δ contribution, and the right the ∇ one. In this example, the correlation coefficient between the two convergence maps, r, is equal to 0.48 at $1.8'$. The cross-correlation coefficient between the guess map (f) and the real one (b) is 0.47. It is 0.37 between the real (b) and Δ (g) maps and goes down to 0.16 for the real (b) and ∇ (h).

gence but also translations and a whole class of a_{nk} realization-dependent complex deformations are indiscernible. Thus, with only knowledge of the B component of the polarization, one cannot, with the first order equation (8), recover the projected mass distribution.

It is worth noting here that this calculation is not in contradiction with the Guzik-Seljak-Zaldarriaga results [10]. In their paper they show that using different statistics, based on polarization measurements, they are able to reconstruct the lens power spectrum of the large-scale structure. Moreover, this reconstruction is hampered by *noise* induced by the autocorrelation of the cosmic microwave background structures. This noise is strongly related to the kernel problem addressed here. They can choose their statistic to reduce this noise to an acceptable level in the power spectrum, yet they cannot reconstruct a shear map.

III. CROSS-CORRELATING CMB MAPS AND WEAK LENSING SURVEYS

A. Motivation

Even with the most precise experiments it is clear that clean detection of B components will be difficult to obtain. The magnetic polarization amplitude induced with such a mechanism is expected to be one order of magnitude below the electric one [17]. Besides, even if we know that there is a window on an angular scale where other secondary effects will not interfere too much with the detection of the lens-induced B [20], little is known about removing the foregrounds [21] to obtain clean maps reconstruction algorithms would require.

These considerations lead us to look for complementary data sets to compare B with. Although the source plane for weak lensing surveys [5] is much closer than for the lensed CMB fluctuations, we expect to have a significant overlapping region in the two redshift lens distributions, so that weak lensing surveys can map a fair fraction of the line-of-sight CMB lenses. Consequently, weak lensing surveys can potentially provide us with shear maps correlated with B, but which have different geometrical degeneracy, noise sources, and systematics than the polarization field.

The correlation strength between the lensing effects at two different redshifts can be evaluated. We define r as the cross-correlation coefficient between two lens planes:

$$r(z_{\rm gal}) = \frac{\langle \kappa \kappa_{\rm gal} \rangle}{\sqrt{\langle \kappa^2 \rangle \langle \kappa_{\rm gal}^2 \rangle}}. \tag{14}$$

In a broad range of realistic cases (see Table I), $r \sim 40\%$. To take advantage of this large overlapping we will consider the quantity that cross-correlates the CMB B field and galaxy surveys. Moreover, cross-correlation observations are expected to be insensitive to noises in weak lensing surveys and in CMB polarization maps. This idea has already been

TABLE I. Values of r, the cross-correlation between two source planes ($z_{\rm gal}$ and $z_{\rm cmb}=1100$), for different models. The adopted filter scale (see Sec. III C for details) is 2 arc min for both the weak lensing survey and cosmic microwave background observations. Non-linear evolution of $P(k)$ has been computed using the Peacock-Dodds method [22].

r coefficient	$z_{\rm gal}=1$	$z_{\rm gal}=2$
EdS, linear	0.42	0.60
$\Omega=0.3,\ \Lambda=0.7,$ linear	0.31	0.50
$\Omega=0.3,\ \Lambda=0.7,$ nonlinear	0.40	0.59

explored for temperature maps [14]. We extend this study here taking advantage of the specific geometrical dependences uncovered in the previous section.

B. Definition of b_Δ and b_∇

The magnetic component of the polarization in Eq. (8) appears to be built from a pure CMB part, which comes from the primordial polarization, and a gravitational lensing part. It is natural to define b in such a way that mimics the $\Delta\hat{B}$ function dependence by replacing the CMB shear field by the galaxy one:

$$\begin{aligned} b &= \epsilon_{ij}(\gamma^i_{\rm gal}\Delta\hat{P}^j + \gamma^i_{{\rm gal},k}\hat{P}^{j,k}) \\ &= \epsilon_{ij}(\gamma^i_{\rm gal}\Delta P^j + \gamma^i_{{\rm gal},k}P^{j,k}) + O(\kappa^2). \end{aligned} \tag{15}$$

In the following, we will label local lensing quantities, such as what one can obtain from lensing reconstruction on galaxy surveys, with a ''gal'' index. This new quantity can be viewed as a guess for the CMB polarization B component if lensing was turned on only in a redshift range matching the depth of galaxy surveys. The correlation coefficient of this guess with the true ΔB field, that is, $\langle\Delta\hat{B}b\rangle$, is expected to be quadratic both in P and in γ and to be proportional to the cross-coefficient r.

For convenience, and in order to keep the objects we manipulate as simple as possible, we will not exactly implement this scheme, as it will lead to uneven angular derivative degrees in the two terms of resulting equations. We can, instead, decompose the effect in the Δ and ∇ parts. These two are not correlated, since their components do not share the same degrees of angular derivation.[2] Hence, we can play the proposed game, considering the two terms of Eq. (8) as if they were two different fields, creating two guess quantities that should correlate independently with the observed B field. Following this idea we build b_Δ as

$$\begin{aligned} b_\Delta &\equiv \epsilon_{ij}\gamma^i_{\rm gal}\Delta\hat{P}^j \\ &= \epsilon_{ij}\gamma^i_{\rm gal}\Delta P^j + O(\kappa^2) \end{aligned} \tag{16}$$

which corresponds to the Δ term in Eq. (8). The amplitude of the cross-correlation between ΔB and b_Δ can easily be estimated. At leading order, we have

$$\langle\Delta\hat{B}b_\Delta\rangle = -2\epsilon_{ij}\epsilon_{kl}\langle\gamma^k\gamma^i_{\rm gal}\rangle\langle\Delta P^l\Delta P^j\rangle. \tag{17}$$

The corresponding ∇ correlation is

$$\langle\Delta\hat{B}b_\nabla\rangle = -2\epsilon_{ij}\epsilon_{kl}\langle\partial_m\gamma^k\partial_n\gamma^i_{\rm gal}\rangle\langle\partial_m P^l\partial_n P^j\rangle, \tag{18}$$

where we have defined

$$b_\nabla \equiv \epsilon_{ij}\partial_k\gamma^i_{\rm gal}\partial_k\hat{P}^j. \tag{19}$$

Figure 4 shows numerical simulations presenting maps of first order $\Delta\hat{B}$, its Δ and ∇ contributions, and the corresponding guess maps one can build with a low-z shear map. The similarities between the top maps and the bottom maps are not striking. Yet under close examination one can recognize individual patterns shared between the maps. This is confirmed by the computation of the correlation coefficient between the maps, which shows significant overlapping, between 50% and 15%, depending the correlation and filtering strategy. The calculations hereafter will evaluate the theoretical correlation structure between maps given in Figs. 4b and 4g, 4h.

For galaxy surveys, the amplification matrix is [23]

$$\begin{aligned} \mathcal{A}^{-1}_{\rm gal}(\vec{\alpha}) - {\rm Id} = &-\int_0^{z_{\rm gal}} {\rm d}\chi w_{\rm gal}(\chi) \\ &\times \int \frac{{\rm d}^3k}{(2\pi)^{3/2}}\delta(\vec{k}){\rm e}^{{\rm i}[k_r\chi+\vec{k}_\perp D(\chi)\vec{\alpha}]} \\ &\times \begin{pmatrix} 1+\cos(2\phi_{k_\perp}) & \sin(2\phi_{k_\perp}) \\ \sin(2\phi_{k_\perp}) & 1-\cos(2\phi_{k_\perp}) \end{pmatrix}, \end{aligned} \tag{20}$$

where $\delta(k)$ is the Fourier transform of the density contrast at redshift $z(\chi)$, w is the lens efficiency function, and $\phi_{k_\perp}$ is the position angle of the transverse wave vector $k_\perp$ in the $k_\perp=(k_x, k_y)$ plane. Assuming a Dirac source distribution, the efficiency function is given by

$$w_{\rm gal}(z) = \frac{3}{2}\Omega_0\frac{D_z D_{z\to z_{\rm gal}}}{aD_{z_{\rm gal}}}. \tag{21}$$

Note that the Fourier components $\delta(k)$ include the density time evolution. They are thus proportional to the growth factor in the linear theory. The time evolution of these components is much more complicated in the nonlinear regime (see [22]).

Then, $b_\natural$ is

$$b_\natural(\vec{\alpha}) = \int^{\chi_{\rm gal}} \mathcal{D}(\chi,\vec{l},\vec{k})\tilde{E}(l)\delta(k)\mathcal{G}^{\rm Ker}_\natural(\vec{l},\vec{k}_\perp), \tag{22}$$

with the integration element defined as

[2]Generically, a random field and its derivative at the same point are not correlated.

$$\mathcal{D}(\chi,\vec{l},\vec{k}) = \mathrm{d}\chi\, w_{\rm gal}(\chi)\frac{\mathrm{d}^3k}{(2\pi)^{3/2}}\frac{\mathrm{d}^2l}{2\pi}\mathrm{e}^{\mathrm{i}[k_r\chi+(\vec{k}_\perp \mathrm{D}(\chi)+\vec{l})\cdot\vec{\alpha}]}$$

[it actually depends on the position of the source plane through the efficiency function $w(z)$] and where $\natural$ stands for either Δ or ∇. The geometrical kernel $\mathcal{G}^{\rm Ker}$ is given by [using Eq. (10)]

$$\mathcal{G}^{\rm Ker}_{\Delta}(\vec{l},\vec{k}) \equiv l^2 \sin 2(\phi_k-\phi_l), \tag{23}$$

$$\mathcal{G}^{\rm Ker}_{\nabla}(\vec{l},\vec{k}) \equiv lk\cos(\phi_k-\phi_l)\sin 2(\phi_k-\phi_l). \tag{24}$$

This function contains all the geometrical structures of the Δ and ∇ terms. We can write the same kind of equation for $\Delta\hat{B}$. Then, the cross-correlation is

$$\begin{aligned}\langle \Delta\hat{B}\, b_\natural(\vec{\alpha})\rangle = -2\int^{\chi_{\rm gal}}&\mathcal{D}(\chi_{\rm gal},\vec{l}_{\rm gal},\vec{k}_{\rm gal})\\ &\times\int^{\chi_{\rm cmb}}\mathcal{D}(\chi_{\rm cmb},\vec{l}_{\rm cmb},\vec{k}_{\rm cmb})\mathcal{G}^{\rm Ker}_\natural(\vec{l}_{\rm gal},\vec{k}_{\rm gal})\\ &\times\mathcal{G}^{\rm Ker}_\natural(\vec{l}_{\rm cmb},\vec{k}_{\rm cmb})\langle\delta(\vec{k}_{\rm gal})\,\delta(\vec{k}_{\rm cmb})\rangle\\ &\times\langle\tilde{E}(\vec{l}_{\rm gal})\tilde{E}(\vec{l}_{\rm cmb})\rangle.\end{aligned} \tag{25}$$

The completion of this calculation requires the use of the small-angle approximation:

$$k\sim k_\perp. \tag{26}$$

Then,

$$\langle\delta(\vec{k}_{\rm gal})\,\delta(\vec{k}_{\rm cmb})\rangle = P(k)\,\delta_{\rm Dirac}(\vec{k}_{\rm gal}+\vec{k}_{\rm cmb}) \tag{27}$$

implies that, and after the radial components have been integrated out,

$$\chi_{\rm gal}=\chi_{\rm cmb}=\chi. \tag{28}$$

We also define the $C_E(l)$ as the angular power spectrum of the E field:

$$\langle\tilde{E}(\vec{l}_{\rm gal})\tilde{E}(\vec{l}_{\rm cmb})\rangle = C_E(l)\,\delta_{\rm Dirac}(\vec{l}_{\rm gal}-\vec{l}_{\rm cmb}). \tag{29}$$

Eventually one gets

$$\begin{aligned}\langle\Delta\hat{B}\, b_\natural(\vec{\alpha})\rangle = -2\int^{z_{\rm gal}}&\mathrm{d}\chi w_{\rm gal}w_{\rm cmb}\\ &\times\int\frac{\mathrm{d}^2k\mathrm{d}^2l}{(2\pi)^4}C_E(l)P(k)\mathcal{G}^{\rm Ker}_\natural(\vec{l},\vec{k})^2.\end{aligned} \tag{30}$$

Then, integrating on the geometrical dependences in $\mathcal{G}^{\rm Ker}_\natural$, we have

$$\begin{aligned}\langle\Delta\hat{B}\, b_\Delta(\vec{\alpha})\rangle &= -2\int^{z_{\rm gal}}\mathrm{d}\chi\, w_{\rm gal}w_{\rm cmb}\int\frac{\mathrm{d}k\mathrm{d}l}{2(2\pi)^2}kl^5C_E(l)P(k)\\ &= -\langle\Delta E^2\rangle\langle\kappa\kappa_{\rm gal}\rangle\end{aligned} \tag{31}$$

and

$$\begin{aligned}\langle\Delta\hat{B}\, b_\nabla(\vec{\alpha})\rangle &= -\int^{z_{\rm gal}}\mathrm{d}\chi\, w_{\rm gal}w_{\rm cmb}\int\frac{\mathrm{d}k\mathrm{d}l}{2(2\pi)^2}k^3l^3C_E(l)P(k)\\ &= -\frac{1}{2}\langle(\vec{\nabla}E)^2\rangle\langle\vec{\nabla}\kappa\cdot\vec{\nabla}\kappa_{\rm gal}\rangle,\end{aligned} \tag{32}$$

implying that, ignoring filtering effects, we are able to measure directly the correlation between lensing effect at $z_{\rm cmb}$ and any $z_{\rm gal}$ a weak lensing survey can access. Since $\Delta\hat{E}=\Delta E[1+O(\kappa)]$, we get, for the Δ type quantity,

$$\langle\Delta\hat{E}^2\rangle = \langle\Delta E^2[1+O(\kappa)]^2\rangle = \langle\Delta E^2\rangle[1+O(\langle\kappa^2\rangle)]. \tag{33}$$

The same holds for ∇. We are then able to construct two quantities insensitive to the normalization of CMB and σ_8:

$$\mathcal{X}_\Delta \equiv \frac{\langle\Delta\hat{B}\, b_\Delta(\vec{\alpha})\rangle}{\langle\Delta\hat{E}^2\rangle\langle\kappa^2_{\rm gal}\rangle} = -\frac{\langle\kappa\kappa_{\rm gal}\rangle}{\langle\kappa^2_{\rm gal}\rangle}\sim -r\sqrt{\frac{\langle\kappa^2\rangle}{\langle\kappa^2_{\rm gal}\rangle}} \tag{34}$$

and

$$\begin{aligned}\mathcal{X}_\nabla &= \frac{\langle\Delta\hat{B}\, b_\nabla(\vec{\alpha})\rangle}{\langle(\vec{\nabla}\hat{E})^2\rangle\langle(\vec{\nabla}\kappa_{\rm gal})^2\rangle}\\ &= -\frac{1}{2}\frac{\langle\vec{\nabla}\kappa\cdot\vec{\nabla}\kappa_{\rm gal}\rangle}{\langle\vec{\nabla}\kappa^2_{\rm gal}\rangle}\sim -\frac{1}{2}r_\nabla\sqrt{\frac{\langle\nabla\kappa^2\rangle}{\langle\nabla\kappa^2_{\rm gal}\rangle}}.\end{aligned} \tag{35}$$

We implicitly defined r_∇ like r but with $\nabla\kappa$ instead of κ:

$$r_\nabla(z_{\rm gal}) = \frac{\langle\vec{\nabla}\kappa\cdot\vec{\nabla}\kappa_{\rm gal}\rangle}{\sqrt{\langle(\nabla\kappa)^2\rangle\langle(\nabla\kappa_{\rm gal})^2\rangle}}. \tag{36}$$

We will see in Sec. III D that they behave very much alike. This result is to be compared with the formula for $\langle\cos(\theta_g)\rangle$ established in [14] where the obtained quantity was going like $r\sqrt{\langle\kappa^2\rangle}$. These calculations, however, have neglected the filtering effects that may significantly affect our conclusions. These effects are investigated in next section.

C. Filtering effects

In above section we conduct our calculations assuming no filtering. Obviously we have to take it into account. We will show here that the results obtained in Sec. III B hold, in certain limits, when filtering effects are included.

In the following, we consider, for simplicity, top-hat filters only. It is expected that other window functions will show very similar behaviors so that this assumption does not limit the scope of our results. Let us call $W(k)$ the top-hat filter function in Fourier space:

$$W(k) \equiv 2\frac{J_1(k)}{k}. \tag{37}$$

J_1 is the first J Bessel function. We will also define $W_i(k)$ as a general function:

$$W_i(k) \equiv 2\frac{J_i(k)}{k}, \tag{38}$$

where J_i is the ith J Bessel function, so that $W = W_1$. Then, if $X(\vec{\alpha})$ is the value of any quantity X at position $\vec{\alpha}$ on the sky, its top-hat-filtered value can be computed as

$$X_{(\theta)}(\vec{\alpha}) = \int \frac{\mathrm{d}^2k}{2\pi}\tilde{X}_k W(k\theta)\mathrm{e}^{\mathrm{i}\vec{k}\cdot\vec{\alpha}}, \tag{39}$$

where $\tilde{X}$ is the X Fourier transform. In the following we will denote $X_{(\theta)}$ the filtered quantity at scale θ.

The tricky thing for $\langle \Delta\hat{B} b_{\natural}\rangle$ is that the CMB part and the low-redshift weak lensing part are *a priori* filtered at different scale. For $\Delta\hat{B}$, which is a measured value, its pure CMB part and its weak lensing part are filtered at the same scale θ. Hence, $\hat{B}$ reads

$$\Delta\hat{B}(\vec{\alpha})_{(\theta)} = -2\int^{\chi_{\mathrm{cmb}}} \mathcal{D}(\chi,\vec{l},\vec{k})\tilde{E}(l)\delta(k)[\mathcal{G}_{\Delta}^{\mathrm{Ker}}(\vec{l},\vec{k}_{\perp}) + \mathcal{G}_{\Delta}^{\mathrm{Ker}}(\vec{l},\vec{k}_{\perp})]W(|\vec{k}_{\perp}D+\vec{l}|\theta). \tag{40}$$

A contrario $b_{\natural}$ is a composite value. The CMB part is still filtered at θ whereas the weak lensing part (which comes from a weak lensing survey of galaxies) is filtered independently at another scale which we denote θ_{gal}. It implies that

$$b_{\natural}(\vec{\alpha})_{(\theta)} = -2\int^{\chi_{\mathrm{gal}}} \mathcal{D}(\chi,\vec{l},\vec{k})\tilde{E}(l)\delta(k)\mathcal{G}_{\natural}^{\mathrm{Ker}}(\vec{l},\vec{k}_{\perp}) \times W(kD\theta_{\mathrm{gal}})W(l\theta). \tag{41}$$

Taking filtering into account, the cross-correlation coefficient becomes

$$\langle \Delta\hat{B}_{(\theta)} b_{\natural(\theta,\theta_{\mathrm{gal}})}\rangle = -2\int^{z_{\mathrm{gal}}} \mathrm{d}\chi\, w_{\mathrm{gal}} w_{\mathrm{cmb}} \int \frac{\mathrm{d}^2k\mathrm{d}^2l}{(2\pi)^4} \times C_E(l)P(k)\mathcal{G}_{\natural}^{\mathrm{Ker}}(\vec{l},\vec{k})W(kD\theta_{\mathrm{gal}}) \times W(l\theta)W(|\vec{k}D+\vec{l}|\theta). \tag{42}$$

It can be shown (from the summation theorems of the Bessel functions) that

$$W_1(|\vec{k}D+\vec{l}|\theta) = -\sum_{i=1} iW_i(kD\theta)W_i(l\theta) \times (-1)^i \frac{\sin i(\phi_k-\phi_l)}{\sin(\phi_k-\phi_l)}. \tag{43}$$

It is then possible to break the $W(|\vec{k}D+\vec{l}|\theta)$ into a sum of $W_i(kD\theta)W_i(l\theta)$ with coefficients that depend on the geometrical properties of our problem. Integrating over the geometrical dependences of $\mathcal{G}_{\natural}^{\mathrm{Ker}}$ leaves us with only a few nonvanishing terms in our sum,

$$\int \mathrm{d}\phi \sin^2(2\phi)\frac{\sin(i\phi)}{\sin\phi} = \begin{cases} \pi & i=1 \text{ or } i=3, \\ 0 & \text{elsewhere,} \end{cases} \tag{44}$$

for the Δ term, and

$$\int \mathrm{d}\phi \cos\phi \sin^2(2\phi)\sin(i\phi)\sin\phi = \begin{cases} \pi/2 & i=1, \\ 3\pi/4 & i=3, \\ \pi/4 & i=5, \\ 0 & \text{elsewhere,} \end{cases} \tag{45}$$

for the ∇ term. Each term can be computed exactly, and it turns out that the terms built from W_i, $i>1$, are always negligible compared to the ones coming from W_1. It implies that we can safely ignore the W_3 and W_5 in both Δ and ∇ expressions; therefore it is reasonable to assume that $W(|\vec{k}D+\vec{l}|\theta) = W(kD\theta)W(l\theta)$. It is expected that other windows, in particular the Gaussian window function, share similar properties. Then, taking into accounts the filtering effects, the equations for the cross-correlations reduce to

$$\langle \Delta\hat{B}_{(\theta)} b_{\Delta(\theta,\theta_{\mathrm{gal}})}\rangle = -\langle \Delta E^2_{(\theta)}\rangle\langle \kappa_{(\theta)}\kappa_{\mathrm{gal}(\theta_{\mathrm{gal}})}\rangle \tag{46}$$

and

$$\langle \Delta\hat{B}_{(\theta)} b_{\nabla(\theta,\theta_{\mathrm{gal}})}\rangle = -\frac{1}{2}\langle \nabla E^2_{(\theta)}\rangle\langle \nabla\kappa_{(\theta)}\nabla\kappa_{\mathrm{gal}(\theta_{\mathrm{gal}})}\rangle, \tag{47}$$

so that our correlation coefficients can be written,

$$\mathcal{X}_{\Delta(\theta,\theta_{\mathrm{gal}})} = -r_{(\theta,\theta_{\mathrm{gal}})}\sqrt{\frac{\langle\kappa^2_{(\theta)}\rangle}{\langle\kappa^2_{\mathrm{gal}(\theta_{\mathrm{gal}})}\rangle}} \tag{48}$$

and

$$\mathcal{X}_{\nabla(\theta,\theta_{\mathrm{gal}})} = -\frac{1}{2}r_{\nabla(\theta,\theta_{\mathrm{gal}})}\sqrt{\frac{\langle\nabla\kappa^2_{(\theta)}\rangle}{\langle\nabla\kappa^2_{\mathrm{gal}(\theta_{\mathrm{gal}})}\rangle}}. \tag{49}$$

The results obtained in Eqs. (34),(35) are thus still formally valid. Actually, Eqs. (48),(49) simply tell us that filtering effects can simply be assumed to act independently on the lensing effects and on the primary cosmic microwave background maps. We are left with two quantities that only reflect the line-of-sight overlapping effects of lensing distortions.

D. Sensitivity to the cosmic parameters

We quickly explore here the behavior of $\mathcal{X}_{\natural}$ in different sets of cosmological parameters. These quantities only depend on weak lensing quantities. Ignoring the Ω_0 dependence in the angular distances and growing factor, one would expect $\langle\kappa^2\rangle$ to scale like Ω_0^2. Yet because of the growth factor, the convergence field exhibits a weaker sensitivity to

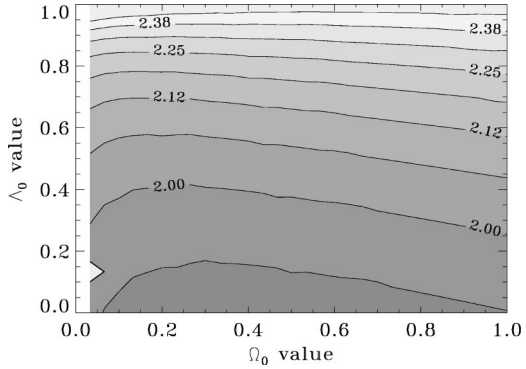

FIG. 5. $\langle \kappa_{(\theta)} \kappa_{\mathrm{gal}(\theta_{\mathrm{gal}})} \rangle / \langle \kappa^2_{\mathrm{gal}(\theta_{\mathrm{gal}})} \rangle$ for a CDM model consistent with the values of (Ω_0, Λ). $\theta = \theta_{\mathrm{gal}} = 2'$.

Ω_0. Assuming $\Lambda = 0$ and a power law spectrum, we know from [23] that $\langle \kappa^2_{\mathrm{gal}} \rangle \propto \Omega_0^{1.66}$ for $z_{\mathrm{gal}} = 1$. The same calculation leads to $\langle \kappa_{\mathrm{cmb}} \kappa_{\mathrm{gal}} \rangle \propto \Omega_0^{1.68}$, $\langle (\nabla \kappa_{\mathrm{gal}})^2 \rangle \propto \Omega_0^{1.91}$, and $\langle \vec{\nabla} \kappa_{\mathrm{cmb}} \cdot \vec{\nabla} \kappa_{\mathrm{gal}} \rangle \propto \Omega_0^{1.915}$. Then, in this limit, the quantities $\mathcal{X}_\natural$ have a very low dependence on Ω_0:

$$\mathcal{X}_\Delta \propto \Omega_0^{0.02} \quad \text{and} \quad \mathcal{X}_\nabla \propto \Omega_0^{0.005}.$$

Eventually, the $\mathcal{X}_\natural$ quantities should exhibit a sizable sensitivity to Λ; changing Λ increases or reduces the size of the optic bench and accordingly the overlapping between κ_{cmb} and κ_{gal}.

Figures 5 and 6 present contour plots of the amplitude of $\mathcal{X}_\Delta$ and $\mathcal{X}_\nabla$ in the (Ω_0, Λ) plane for CDM models. They show the predicted low Ω_0 sensitivity and the expected Λ dependence. Both figures are very alike. This is due to the fact that the dominant features are contained in the efficiency function dependences on the angular distances.

E. Cosmic variance

In previous sections we looked at the sensitivity of observable quantities which mixed galaxy weak lensing surveys and CMB polarization detection. It is very unlikely that both surveys will be able to cover, with good resolution and low foreground contamination, a large fraction of the sky. It seems, however, reasonable to expect to have at our disposal patches of at least a few hundred square degrees. The issue

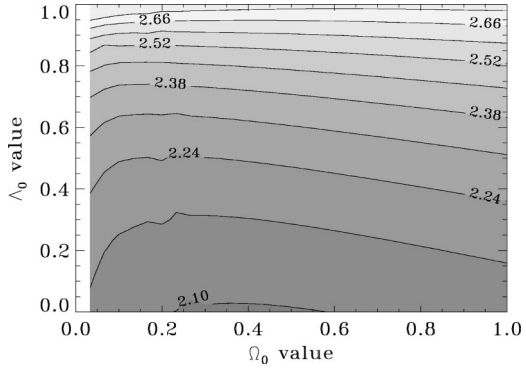

FIG. 6. $\langle \vec{\nabla} \kappa_{(\theta)} \cdot \vec{\nabla} \kappa_{\mathrm{gal}(\theta_{\mathrm{gal}})} \rangle / \langle (\vec{\nabla} \kappa_{\mathrm{gal}(\theta_{\mathrm{gal}})})^2 \rangle$ for a CDM model. $\theta = \theta_{\mathrm{gal}} = 2'$.

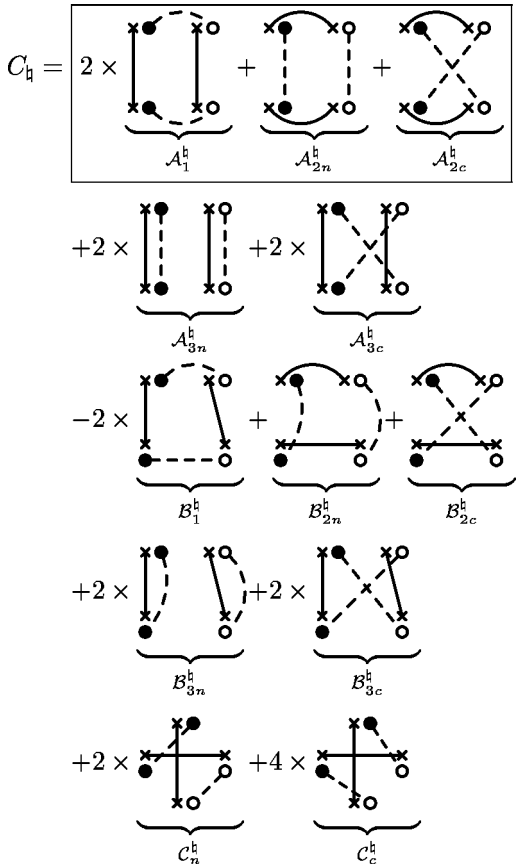

FIG. 7. Diagrammatic representation of the terms contributing to the cosmic variance of the correlation coefficients. In this representation the vertex x● represents $\Delta\hat{B}$; the crosses stand for the ΔP part, the circles for γ_{cmb}. The other vertex x○ represents any $b_\natural$; the open circles stand for γ_{gal}. The solid lines connect ΔP terms and the dashed ones the γ's.

we address in this section is to estimate the cosmic variance of such a detection in joint surveys in about 100 square degrees.

The computation of cosmic variance is a classical problem in cosmological observation [24]. A natural estimate for an ensemble average $\langle X \rangle$ is its geometrical average. If the survey has size Σ, then

$$\overline{X} = \frac{1}{\Sigma} \int_\Sigma \mathrm{d}^2 \alpha X(\vec{\alpha}). \tag{50}$$

For a compact survey with circular shape of radius Ξ we formally have

$$\overline{X} = \int \frac{\mathrm{d}^2 k}{2\pi}, \tilde{X}(\vec{k}) W(k\Xi). \tag{51}$$

For the sake of simplicity this is what we use in the following but we will see that the shape of the survey has no significant consequences.

Taking $\overline{X}$ as an estimate of $\langle X \rangle$ (the ensemble average of X) leads to an error of the order of $\sqrt{\langle \overline{X}^2 \rangle - \langle \overline{X} \rangle^2}$ which usually scales like $1/\sqrt{\Sigma}$ if the survey is large enough.

When we are measuring $\mathcal{X}_\natural$ on a small patch of sky, we are apart from the statistical value by the same kind of error. We can neglect the errors on $\langle \Delta\hat{E}^2\rangle$, $\langle(\nabla\hat{E})^2\rangle$, $\langle(\nabla\kappa_{\rm gal})^2\rangle$ and $\langle\kappa_{\rm gal}^2\rangle$; those may not be the dominant source of the discrepancy and can even be measured on wider and independent samples. The biggest source of error is the measure of $\langle\Delta\hat{B}b_\natural\rangle$. It is given by

$$C_\natural=\sqrt{\langle(\overline{\Delta\hat{B}b_\natural}-\overline{\Delta\hat{B}}\,\overline{b_\natural})^2\rangle-\langle\overline{\Delta\hat{B}b_\natural}-\overline{\Delta\hat{B}}\,\overline{b_\natural}\rangle^2}. \quad (52)$$

Computation of Eq. (52) is made easier if we write explicitly the geometrical average as a summation over N measurement points (N can be as large as we want),

$$\overline{X}=\frac{1}{N}\sum_{i=1}^{N}X(\theta_i); \quad (53)$$

we then developed Eq. (52), and replaced the ensemble average of the summation sign by the geometrical average over the survey size. We are left with a sum of correlators containing eight fields taken at two, three, and four different points. The calculations can be carried out analytically if we assume that all our fields follow Gaussian statistics, which is reasonable at the scale we are working on. In that case, indeed, we can take advantage of the Wick theorem to contract each of the eight field correlators in products of two-point correlation functions. By definition, Eq. (52) contains only connected correlators; moreover, the ensemble averages $\langle\Delta\hat{B}\rangle$ and $\langle b_\natural\rangle$ vanish, and therefore only a small fraction of correlators among all the possible combination of the eight fields survive. We can use a simple diagrammatic representation to describe their geometrical shape. All the nonvanishing terms in $C_\natural$ are given in Fig. 7. Each line between two vertex represents a two-point correlation function such as $\langle X(\vec{\alpha}_1)X(\vec{\alpha}_2)\rangle$, and the different symbols at the vertex correspond to different X fields (the crosses stand for ΔP, the solid circles for $\gamma_{\rm cmb}$, and the open circles for $\gamma_{\rm gal}$). The $\mathcal{A}$ terms represent terms where the two top (and the two bottom) ΔB and $b_\natural$ are taken at the same point, but top and bottom fields are not at the same place. The $\mathcal{B}$ terms are three-point diagrams: the top ΔB and $b_\natural$ are at the same point whereas the right and left bottom vertexes are at two different locations. The $\mathcal{C}$ terms are four-point diagrams, where each vertex is at a different point. To illustrate our notation, let us write $\mathcal{B}_{2c}^\natural$ as an example:

$$\mathcal{B}_{2c}^\natural=\langle\gamma_{\rm cmb}(\vec{\alpha}_1)\gamma_{\rm gal}(\vec{\alpha}_2)\rangle\langle\gamma_{\rm gal}(\vec{\alpha}_3)\gamma_{\rm cmb}(\vec{\alpha}_1)\rangle \times\langle\Delta P(\vec{\alpha}_1)\Delta P(\vec{\alpha}_1)\rangle\langle\Delta P(\vec{\alpha}_2)\Delta P(\vec{\alpha}_3)\rangle. \quad (54)$$

We only focus on the calculation of the $\mathcal{A}$ terms because we can use the approximation that

$$\mathcal{A}\gg\mathcal{B}\gg\mathcal{C}. \quad (55)$$

Indeed, in perturbative theory, if the survey is large enough, the n-point correlation function naturally dominates over the $(n+1)$ point correlation function. This is true as long as the local variance is much bigger than the autocorrelation at survey scale and we assume the surveys are still large enough to be in this case.

The general expression for any $\mathcal{A}$ diagram is

$$\begin{aligned}\mathcal{A}_i^\natural=4\int^{\rm cmb}&\mathcal{D}(\chi_{\rm cmb1},\vec{l}_{\rm cmb1},\vec{k}_{\rm cmb1})\mathcal{D}(\chi_{\rm cmb2},\vec{l}_{\rm cmb2},\vec{k}_{\rm cmb2})\\ &\times\int^{\rm gal}\mathcal{D}(\chi_{\rm gal1},\vec{l}_{\rm gal1},\vec{k}_{\rm gal1})\mathcal{D}(\chi_{\rm gal2},\vec{l}_{\rm gal2},\vec{k}_{\rm gal2})\mathcal{G}_\natural^{\rm Ker}(\vec{l}_{\rm cmb1},\vec{k}_{\rm cmb1_\perp})\mathcal{G}_\natural^{\rm Ker}(\vec{l}_{\rm cmb2},\vec{k}_{\rm cmb2_\perp})\mathcal{G}_\natural^{\rm Ker}(\vec{l}_{\rm gal1},\vec{k}_{\rm gal1_\perp})\\ &\times\mathcal{G}_\natural^{\rm Ker}(\vec{l}_{\rm gal2},\vec{k}_{\rm gal2_\perp})\mathcal{M}_i\langle\vec{k}_i|\vec{l}_j\rangle W(|\vec{k}_{\rm cmb1_\perp}D+\vec{l}_{\rm cmb1}|\theta)W(|\vec{k}_{\rm cmb2_\perp}D+\vec{l}_{\rm cmb2}|\theta)W(k_{\rm gal1_\perp}D_1\theta_{\rm gal})W(l_{\rm gal1}\theta)\\ &\times W(k_{\rm gal2_\perp}D_2\theta_{\rm gal})W(l_{\rm gal2}\theta)W(|\vec{k}_{\rm gal1_\perp}D_1+\vec{l}_{\rm gal1}+\vec{k}_{\rm cmb1_\perp}D_1+\vec{l}_{\rm cmb1}|\Xi)W(|\vec{k}_{\rm gal2_\perp}D_2+\vec{l}_{\rm gal2}+\vec{k}_{\rm cmb2_\perp}D_2+\vec{l}_{\rm cmb2}|\Xi),\end{aligned} \quad (56)$$

where $\mathcal{M}_i$ gives the two-point correlations associated with the lines of the diagram. For example,

$$\mathcal{M}_1=\langle\delta(\vec{k}_{\rm gal1})\delta(\vec{k}_{\rm cmb1})\rangle\langle\delta(\vec{k}_{\rm gal2})\delta(\vec{k}_{\rm cmb2})\rangle\langle\tilde{E}(l_{\rm gal1})\tilde{E}(l_{\rm gal2})\rangle\langle\tilde{E}(l_{\rm cmb1})\tilde{E}(l_{\rm cmb2})\rangle. \quad (57)$$

We explicate in the following the computation of $\mathcal{A}_1^\natural$. The other terms follow the same treatment or can be neglected. The lines in the $\mathcal{A}_1^\natural$ diagram give us the relations

$$\vec{k}_{\rm cmb1}=-\vec{k}_{\rm gal1}=\vec{k}_1,\quad \vec{k}_{\rm cmb2}=-\vec{k}_{\rm gal2}=\vec{k}_2,\quad \vec{l}_{\rm cmb1}=-\vec{l}_{\rm cmb2}=\vec{l}_{\rm cmb},\quad \vec{l}_{\rm gal1}=-\vec{l}_{\rm gal2}=\vec{l}_{\rm gal}. \quad (58)$$

Then, using these relations and the small angular approximation, we have

$$\mathcal{A}_1^{\natural}=4\int^{\rm gal}\mathrm{d}\chi_1\mathrm{d}\chi_2 w_{\rm cmb1}w_{\rm gal1}w_{\rm cmb2}w_{\rm gal2}\int\frac{\mathrm{d}^2k_1\mathrm{d}^2k_2}{(2\pi)^4}\frac{\mathrm{d}^2l_{\rm gal}\mathrm{d}^2l_{\rm cmb}}{(2\pi)^4}C_E(l_{\rm gal})C_E(l_{\rm cmb})P(k_1)P(k_2)\mathcal{G}_{\natural}^{\rm Ker}(\vec{l}_{\rm cmb},\vec{k}_1)$$
$$\times\mathcal{G}_{\natural}^{\rm Ker}(-\vec{l}_{\rm cmb},\vec{k}_2)\mathcal{G}_{\natural}^{\rm Ker}(\vec{l}_{\rm gal},-\vec{k}_1)\mathcal{G}_{\natural}^{\rm Ker}(-\vec{l}_{\rm gal},-\vec{k}_2)W(|\vec{k}_1D+\vec{l}_{\rm cmb}|\theta)W(|\vec{k}_2D+\vec{l}_{\rm cmb}|\theta)$$
$$\times W(k_1D\theta_{\rm gal})W(k_2D\theta_{\rm gal})W^2(l_{\rm gal}\theta)W^2(|\vec{l}_{\rm gal}+\vec{l}_{\rm cmb}|\Xi). \tag{59}$$

We apply the decomposition of $W_1(|\vec{k}D(\chi)+\vec{l}|\theta)$ we used in Eq. (43). The geometry of our problem is the same and the result (44) still holds for the terms in $W_1(|\vec{k}_1D(\chi_1)+\vec{l}_{\rm cmb}|\theta)$ and $W_1(|\vec{k}_2D(\chi_2)+\vec{l}_{\rm cmb}|\theta)$. This, however, is not true for $W_1^2(|\vec{l}_{\rm gal}+\vec{l}_{\rm cmb}|\Xi)$ for which the application of the resummation theorem does not bring any simplification. Then, neglecting all W_3 parts and after integration on ϕ_{k_i}, for the Δ term, we have

$$\mathcal{A}_1^{\Delta}=\int^{\rm gal}\mathrm{d}\chi_1\mathrm{d}\chi_2 w_{\rm cmb1}w_{\rm gal1}w_{\rm cmb2}w_{\rm gal2}\int\frac{\mathrm{d}k_1\mathrm{d}k_2}{(2\pi)^2}\frac{\mathrm{d}^2l_{\rm gal}\mathrm{d}^2l_{\rm cmb}}{(2\pi)^4}l_{\rm gal}^4l_{\rm cmb}^4k_1k_2C_E(l_{\rm gal})C_E(l_{\rm cmb})P(k_1)P(k_2)$$
$$\times W^2(|\vec{l}_{\rm gal}+\vec{l}_{\rm cmb}|\Xi)\cos^2 2(\phi_{l_{\rm cmb}}-\phi_{l_{\rm gal}})W(k_1D\theta_{\rm gal})W(k_2D\theta_{\rm gal})W^2(l_{\rm gal}\theta)W(k_1D\theta)W(k_2D\theta)W^2(l_{\rm cmb}\theta). \tag{60}$$

Note that for the evaluation of the ∇ part, using the same kind of method, we obtain the same equation as Eq. (60) where $l_{\rm gal}^4l_{\rm cmb}^4$ is replaced by $l_{\rm gal}^2l_{\rm cmb}^2k_1^2k_2^2/2$.

We can get rid of the remaining $W^2(|\vec{l}_{\rm gal}+\vec{l}_{\rm cmb}|\Xi)$ with another approximation. The power spectrum $C_E(l)$ favors large values of l whereas $W^2(|\vec{l}_{\rm gal}+\vec{l}_{\rm cmb}|\Xi)$ will be nonzero for $|\vec{l}_{\rm gal}+\vec{l}_{\rm cmb}|\sim 1/\Xi$. Then for a typical survey size of about 100 square degrees, $|\vec{l}_{\rm gal}+\vec{l}_{\rm cmb}|\ll l_i$ and we can assume $\vec{l}_{\rm gal}\sim-\vec{l}_{\rm cmb}$ and $\vec{l}_{\rm gal}+\vec{l}_{\rm cmb}=\vec{\epsilon}$. In this limit, $\cos^2 2(\phi_{l_{\rm cmb}}-\phi_{l_{\rm gal}})=1$ and $\mathcal{A}_1^{\natural}$ can be written

$$\mathcal{A}_1^{\Delta}=\int\frac{l\,\mathrm{d}l}{(2\pi)^2}l^8C_E^2(l)W^4(l\theta)\int\frac{\mathrm{d}^2\epsilon}{2\pi}l^8W_1^2(\epsilon\Xi)$$
$$\times\left[\int^{\rm gal}\mathrm{d}\chi w_{\rm cmb}w_{\rm gal}\int\frac{k\,\mathrm{d}k}{2\pi}P(k)W(kD\theta)W(kD\theta_{\rm gal})\right]^2, \tag{61}$$

which is essentially the cosmic variance of $\langle\Delta E^2\rangle$ for the Δ part and of $\langle(\nabla E)^2\rangle$ for the ∇ one [where l^8 in Eq. (61) is replaced by $l^4k_1^2k_2^2/2$]. Finally we have

$$\frac{\mathcal{A}_1^{\Delta}}{\langle B_{(\theta)}b_{\Delta(\theta,\theta_{\rm gal})}\rangle^2}=\frac{2\pi}{\Sigma}\frac{\int\mathrm{d}l\,l^9C_E^2(l)W_1^4(l\theta)}{\left[\int\mathrm{d}l\;l^5C_E(l)W_1^2(l\theta)\right]^2}$$
$$\propto\text{cosmic variance of }\Delta E^2, \tag{62}$$

where $\Sigma=\pi\Xi^2$ in case of a disk-shaped survey. We show in Fig. 8 numerical results for a 100 deg^2 survey although the numerical calculations were done with a Gaussian window function instead of a top hat.

Numerically, for $\theta=10'$, we get

$$\frac{\mathcal{A}_1^{\natural}}{\langle B_{(\theta)}b_{\natural(\theta,\theta_{\rm gal})}\rangle^2}\sim\frac{(3.7\%)^2}{\Sigma/100\ \ \rm deg^2}. \tag{63}$$

We expect that for the same reasons the $\mathcal{A}_2^{\natural}$ terms will be dominated by the weak lensing variance. Yet a correct evaluation here is harder to reach. We have made this estimation within the framework of a power law $P(k)$. With this simplification in hand, we can write, for $\mathcal{A}_{2n}^{\natural}$ (we focus only the Δ part, but the same discussion holds for the ∇ observable),

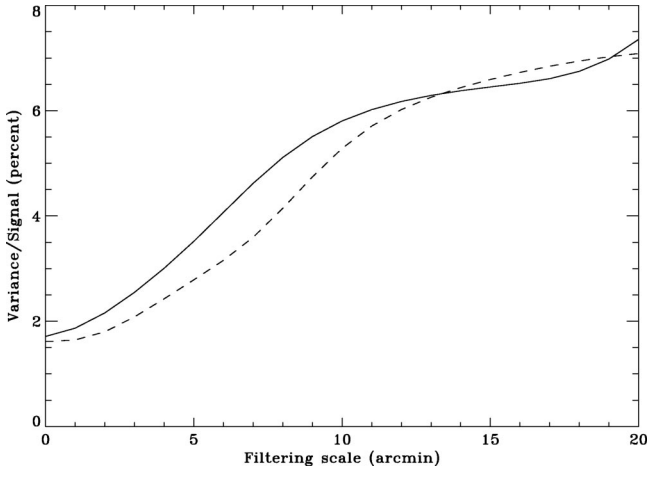

FIG. 8. Comparison between $\sqrt{2A_1^{\Delta}/\text{signal}_{\Delta}}$ (solid line) and $\sqrt{2A_1^{\nabla}/\text{signal}_{\nabla}}$ (dashed line). The C_l are from a $\Omega=0.3$, $\Lambda=0.7$ model. The survey size is 100 deg^2, and Gaussian filters were used.

TABLE II. Values of the cosmic variance of $\langle\kappa^2\rangle$ and $\langle(\vec{\nabla}\kappa)^2\rangle$ for different models and different filtering radius. The size of the survey is 100 deg^2. For the $\Omega_0=0.3$ ($\Omega_0=1$) model, we use five (seven) independent ray-tracing realizations (see [25]) to estimate the cosmic variance in a 9 deg^2 survey, which is then rescaled to the cosmic variance we should obtain for a 100 deg^2 survey. Given the low number of realizations, the values here can only be used as a good estimation of the order of magnitude of CosVar($\langle\kappa^2\rangle$) and CosVar($\langle(\vec{\nabla}\kappa)^2\rangle$). It also seems, from these figures, that the cosmic variance of $\langle(\vec{\nabla}\kappa)^2\rangle$ is more degraded by the difference in filtering beams than the other.

	CosVar($\langle\kappa^2\rangle$)		CosVar($\langle(\vec{\nabla}\kappa)^2\rangle$)	
	$\Omega_0=0.3$	$\Omega_0=1$	$\Omega_0=0.3$	$\Omega_0=1$
$\theta=5', \theta_{\rm gal}=2.5'$	2.94%	1.86%	2.88%	2.07%
$\theta=5', \theta_{\rm gal}=5'$	3.02%	1.87%	2.23%	1.75%
$\theta=10', \theta_{\rm gal}=5'$	3.54%	2.03%	4.25%	3.02%

$$\frac{\mathcal{A}^{\Delta}_{2n}}{\langle B_{(\theta)} b_{\Delta(\theta,\theta_{\rm gal})}\rangle^2} = \frac{1}{r^2}\int {\rm d}^2k_1 {\rm d}^2k_2 P(k_1)P(k_2)\cos^2(\phi_{k_1}-\phi_{k_2}) \times \frac{W_1^2(k_1\theta)W_1^2(k_2\theta_{\rm gal})W_1^2(|\vec{k}_1+\vec{k}_2|\Xi)}{\left[\int {\rm d}^2k P(k) W_1(k\theta) W_1(k\theta_{\rm gal})\right]^2}. \quad (64)$$

The last integral behaves essentially like the cosmic variance of $\langle\kappa^2\rangle$. More exactly, it goes like $1/\sqrt{2}$ of this variance. It should even be smaller, because of the extra $\cos^2$ factor. We evaluated this cosmic variance using the ray-tracing simulations described in [25]. These simulations provide us with realistic convergence maps (for the cosmological models we are interested in) with a resolution of $0.1'$, and a survey size of 9 deg^2. The sources have been put at a redshift unity, and the ray lights are propagated through a simulated Universe whose density field has been evolved from an initial CDM power spectrum. The measured cosmic variance of $\langle\kappa_{(\theta)}\kappa_{(\theta_{\rm gal})}\rangle$ is about 3% (see Table II) when filtered at scales $\theta_{\rm gal}=5'$ and $\theta=10'$ for a $\Omega_0=0.3$ cosmology.

An estimation of $\mathcal{A}^{\Delta}_{2n}$ is then given by

$$\frac{\mathcal{A}^{\Delta}_{2n}}{\langle B_{(\theta)} b_{\Delta(\theta,\theta_{\rm gal})}\rangle^2} \sim \left(\frac{2.12\%}{r}\right)^2 \frac{1}{\Sigma/100\ \ {\rm deg}^2}. \quad (65)$$

Since r_∇ is very comparable to r, we very roughly estimate $\mathcal{A}^{\nabla}_{2n}$:

$$\frac{\mathcal{A}^{\nabla}_{2n}}{\langle B_{(\theta)} b_{\nabla(\theta,\theta_{\rm gal})}\rangle^2} \sim \left(\frac{2.12\%}{r}\right)^2 \frac{1}{\Sigma/100\ \ {\rm deg}^2}. \quad (66)$$

The same considerations give

TABLE III. Values of the cosmic variance of $\mathcal{X}_\natural$. The survey size is 100 deg^2. We used the results presented in Table II and Fig. 8. The $r_\natural$ parameters are assumed to be equal and set to 0.4. We did not take into account the filtering effects in the definition of r. The difference due to the filtering correction is small, though. From this estimation, we can expect a cosmic variance for $\mathcal{X}_\natural$ of less than 10% for realistic scenarios.

	CosVar($\mathcal{X}_\Delta$)		CosVar($\mathcal{X}_\nabla$)	
	$\Omega_0=0.3$	$\Omega_0=1$	$\Omega_0=0.3$	$\Omega_0=1$
$\theta=5', \theta_{\rm gal}=2.5'$	6.44%	4.77%	6.06%	4.72%
$\theta=5', \theta_{\rm gal}=5'$	6.58%	4.79%	4.99%	4.23%
$\theta=10', \theta_{\rm gal}=5'$	8.71%	6.73%	9.49%	7.62%

$$\frac{\mathcal{A}^{\natural}_{2n}}{\langle B_{(\theta)} b_{\natural(\theta,\theta_{\rm gal})}\rangle^2} = \frac{(2.12\%)^2}{\Sigma/100\ \ {\rm deg}^2}. \quad (67)$$

There is no r dependence here; the diagram cross-correlates $\kappa_{\rm cmb}$ and $\kappa_{\rm gal}$.

We can approximate the remaining $\mathcal{A}$ terms. They should be smaller than the former. We have

$$\mathcal{A}^{\natural}_{3n} \sim \frac{1}{r^2_\natural}\frac{(2.12\%\times 3.7\%)^2}{\Sigma/100\ \ {\rm deg}^2}\langle B_{(\theta)} b_{\natural(\theta,\theta_{\rm gal})}\rangle^2 \ll \mathcal{A}^{\natural}_{2n}$$

and

$$\mathcal{A}^{\natural}_{3c} \sim \frac{(2.12\%\times 3.7\%)^2}{\Sigma/100\ \ {\rm deg}^2}\langle B_{(\theta)} b_{\natural(\theta,\theta_{\rm gal})}\rangle^2 \ll \mathcal{A}^{\natural}_{2c}.$$

Then, only the $\mathcal{A}^{\natural}_1$ and $\mathcal{A}^{\natural}_2$ terms (boxed in Fig. 7) contribute substantially to the cosmic variance of $\mathcal{X}_\natural$. Since $\mathcal{A}^{\natural}_1$ and $\mathcal{A}^{\natural}_2$ are, respectively, the cosmic variance of $\langle\Delta E^2\rangle$ (respectively, $\langle(\vec{\nabla}E)^2\rangle$) and of $\langle\kappa^2\rangle$ (respectively, $\langle(\vec{\nabla}\kappa)^2\rangle$), we can write the variance of $\mathcal{X}_\natural$ as

$${\rm CosVar}(\mathcal{X}_\Delta) = {\rm CosVar}(\langle\Delta E^2\rangle) + \left(\frac{1+r^2}{2r^2}\right){\rm CosVar}(\langle\kappa^2\rangle). \quad (68)$$

and

$${\rm CosVar}(\mathcal{X}_\nabla) = {\rm CosVar}(\langle(\vec{\nabla}E)^2\rangle) + \left(\frac{1+r^2_\nabla}{2r^2_\nabla}\right){\rm CosVar}(\langle(\vec{\nabla}\kappa)^2\rangle). \quad (69)$$

Table III presents numerical results for various filtering scenarios and models.

The two quantities b_Δ and b_∇ lead to similar cosmic variances that are rather small. Obviously it would be even better to use $b=b_\Delta+b_\nabla$. For such a quantity the resulting cosmic variance for the cross-correlation coefficient should even be smaller, by a factor of $\sqrt{2}$, although a detailed analysis is made complicated because of the complex correlation patterns it contains.

IV. CONCLUSION

We have computed a first order mapping that describes, in real space, the weak lensing effects on the CMB polarization. In particular we derived the explicit mathematical relation between the primary CMB polarization and the shear field at leading order in the lens effect. It demonstrates that a *B* component of the polarization field can be induced by lens couplings. We have shown, however, that the *B* map alone cannot lead to a nonambiguous reconstruction of the projected mass map.

Nonetheless, the *B* component can potentially exhibit a significant correlation signal with local weak lensing surveys. This opens a new window for detecting lens effects on CMB maps. In particular, and contrary to previous studies involving the temperature maps alone, we found that such a correlation can be measured with a rather high signal-to-noise ratio even in surveys of rather modest size and resolution. Anticipating data sets that should be available in the near future ($100\ \mathrm{deg}^2$ survey, with $5'$ resolution for galaxy survey and $10'$ Gaussian beam size for CMB polarization detection), we have obtained a cosmic variance around 8%. Needless to say, this estimation does not take into account systematics and possible foreground contaminations. It shows anyway that cosmic microwave background polarization contains a precious window for studying the large-scale mass distribution and consequently putting new constraints on the cosmological parameters.

In this paper we have investigated specific quantities that would be accessible to observations. They both would permit one to put a constraint on the cosmological constant. The simulated maps we presented here are only of illustrative interest. We plan to complement this study with extensive numerical experiments to validate our results (in particular on the cosmic variance) and explore the effect of realistic ingredients we did not include in our simple analytical framework: shear non-Gaussianity, lens-lens coupling, and so forth.

ACKNOWLEDGMENTS

We thank B. Jain, U. Seljak, and S. White for the use of their ray-tracing simulations. K.B. and F.B. thank CITA for hospitality and L.v.W. is thankful to SPhT Saclay for hospitality. We are all grateful to the TERAPIX data center located at IAP for providing us computing facilities.

APPENDIX: POWER SPECTRUM OF ΔB AND THE Δ AND ∇ TERMS

The aim of this appendix is to succinctly present the computation of the power spectrum of ΔB and the different terms that contribute to it as shown in Fig. 3. Unlike previous literature on the subject [9,15] we do not need to compute the second order development of the lens effect if we restrict our computations to the power spectrum of the *B* field. The reason why is that assuming that the primordial *B* polarization is null, the second order of the lens effect will have a null contribution to the *B* power spectrum at leading order.

Using Eq. (8), we have

$$\begin{aligned}\langle \Delta\hat{B}(\vec{\alpha}_1)\Delta\hat{B}(\vec{\alpha}_2)\rangle = &\langle \mathcal{B}_\Delta(\vec{\alpha}_1)\mathcal{B}_\Delta(\vec{\alpha}_2)\rangle + \langle \mathcal{B}_\nabla(\vec{\alpha}_1)\mathcal{B}_\nabla(\vec{\alpha}_2)\rangle \\ &+ \langle \mathcal{B}_\Delta(\vec{\alpha}_1)\mathcal{B}_\nabla(\vec{\alpha}_2)\rangle \\ &+ \langle \mathcal{B}_\nabla(\vec{\alpha}_1)\mathcal{B}_\Delta(\vec{\alpha}_2)\rangle, \end{aligned} \tag{A1}$$

where the $\mathcal{B}_\natural$ are the Δ and ∇ parts of ΔB. Then, one can calculate $C_l^{\Delta B}$, the power spectrum of ΔB,

$$C_l^{\Delta B} = C_l^{\Delta\Delta} + C_l^{\nabla\nabla} + 2C_l^{\Delta\nabla}, \tag{A2}$$

where $C_l^{\Delta\Delta}$ (respectively, $C_l^{\nabla\nabla}$) is the power spectrum of the Δ term (∇ term) and $C_l^{\Delta\nabla}$ is the cross-correlation at scale l of the Δ and ∇ terms. The latter must sum up to zero, so that $\langle \mathcal{B}_\nabla \mathcal{B}_\Delta\rangle = 0$. Using the notations of Sec. III, we have

$$\begin{aligned}\langle \mathcal{B}_\sharp(\vec{\alpha}_1)\mathcal{B}_\natural(\vec{\alpha}_2)\rangle &= \int \frac{\mathrm{d}^2 l}{(2\pi)^2} C_l^{\sharp\natural} \mathrm{e}^{\mathrm{i}\vec{l}\cdot(\vec{\alpha}_2-\vec{\alpha}_1)} \\ &= \int \frac{\mathrm{d}^2 k \mathrm{d}^2 h}{(2\pi)^4} C_E(h)\overline{P}(k)\mathrm{e}^{\mathrm{i}(\vec{k}+\vec{h})\cdot(\vec{\alpha}_2-\vec{\alpha}_1)} \\ &\quad \times \mathcal{G}_\natural^{\mathrm{Ker}}(\vec{h},\vec{k})\mathcal{G}_\sharp^{\mathrm{Ker}}(\vec{h},\vec{k}), \end{aligned} \tag{A3}$$

where we have assumed that $\overline{P}(k)$ take into account the line-of-sight integration. We are left with the simple equation

$$C_l^{\sharp\natural} = \int \frac{\mathrm{d}^2 h}{(2\pi)^2} C_E(h)\overline{P}(|\vec{l}-\vec{h}|)\mathcal{G}_\natural^{\mathrm{Ker}}(\vec{h},\vec{l}-\vec{h})\mathcal{G}_\sharp^{\mathrm{Ker}}(\vec{h},\vec{l}-\vec{h}).$$

Figure 3 presents $C_l^{\Delta\Delta}$, $C_l^{\nabla\nabla}$, and $C_l^{\Delta B}$ obtained with these equations.

[1] Among the current and future high-precision observations, the most promising are probably the BOOMERanG balloon experiment [P. de Bernardis *et al.*, New Astron. Rev. **43**, 281 (1999)]; the MAP satellite mission [C.L. Bennett *et al.*, Am. Astron. Soc. Meeting **187**, 7109 (1995)]; and Planck Surveyor satellite mission [M. Bersanelli *et al.*, Report No. COBRAS/SAMBA on the phase A study, ESA Report No. D/SCI(96)3].

[2] M. Zaldarriaga, D. Spergel, and U. Seljak, Astrophys. J. **488**, 1 (1997); G. Efstathiou and J. R. Bond, Mon. Not. R. Astron. Soc. **304**, 75 (1999).

[3] S. Perlmutter *et al.*, Astrophys. J. **517**, 565 (1999); A. G. Riess *et al.*, Astron. J. **116**, 1009 (1998).

[4] A. Aguirre, Astrophys. J. **525**, 583 (1999); T. Totani and C. Kobayashi, Astrophys. J. Lett. **526**, 65 (1999); M. Livio, astro-ph/9903264; K. Nomoto, astro-ph/9907386; P. Valageas, Astron. Astrophys. **354**, 767 (2000).

[5] Y. Mellier, Annu. Rev. Astron. Astrophys. **37**, 127 (1999).

[6] A. Blanchard and J. Schneider, Astron. Astrophys. **184**, 1 (1987); U. Seljak, Astrophys. J. **463**, 1 (1996).

[7] F. Bernardeau, Astron. Astrophys. **324**, 15 (1997); M. Zaldar-

riaga, Phys. Rev. D **62**, 063510 (2000).
[8] F. Bernardeau, Astron. Astrophys. **338**, 767 (1998).
[9] U. Seljak and M. Zaldarriaga, Phys. Rev. Lett. **82**, 2636 (1999); M. Zaldarriaga and U. Seljak, Phys. Rev. D **58**, 023003 (1998).
[10] J. Guzik, U. Seljak, and M. Zaldarriaga, Phys. Rev. D **62**, 043517 (2000).
[11] M. Zaldarriaga and U. Seljak, Phys. Rev. D **58**, 023003 (1998).
[12] K. Benabed and F. Bernardeau, Phys. Rev. D **61**, 123510 (2000).
[13] M. Suginohara, T. Suginohara, and D. N. Spergel, Astrophys. J. **495**, 511 (1998); H. V. Peiris and D. N. Spergel, *ibid.* **540**, 605 (2000).
[14] L. van Waerbeke, F. Bernardeau, and K. Benabed, Astrophys. J. **540**, 14 (2000).
[15] W. Hu, Phys. Rev. D **62**, 043007 (2000).
[16] V. Faraoni, Astron. Astrophys. **272**, 385 (1993).
[17] U. Seljak, Astrophys. J. **482**, 6 (1997); W. Hu and M. White, New Astron. **2**, 323 (1997); J. Lesgourgues, D. Polarski, S. Prunet, and A. A. Starobinsky, Astron. Astrophys. **359**, 414 (2000).
[18] A. Riazuelo, Ph.D. thesis, University of Paris 11, 2000.
[19] L. van Waerbeke, F. Bernardeau, and Y. Mellier, astro-ph/9807007.
[20] W. Hu, Astrophys. J. **529**, 12 (2000).
[21] F. R. Bouchet, S. Prunet, and S. K. Sethi, Mon. Not. R. Astron. Soc. **302**, 663 (1999); S. Prunet, S. K. Sethi, and F. R. Bouchet, Mon. Not. R. Astron. Soc. **314**, 348 (2000).
[22] J. A. Peacock and S. J. Dodds, Mon. Not. R. Astron. Soc. **280**, L19 (1996).
[23] F. Bernardeau, L. van Waerbeke, and Y. Mellier, Astron. Astrophys. **322**, 1 (1997).
[24] M. Srednicki, Astrophys. J. Lett. **416**, 1 (1993).
[25] B. Jain, U. Seljak, and S. White, Astrophys. J. **530**, 547 (2000).